THE JOURNAL OF PHYSICAL CHEMISTRY C
A JOURNAL OF THE AMERICAN CHEMICAL SOCIETY

pubs.acs.org/JPCC

Article

Reactions of Ions with Adsorbed $Me_3PtCpMe$: The Role of Ion Identity

Mohammed K. Abdel-Rahman, Patrick M. Eckhert, Lisa McElwee-White, and D. Howard Fairbrother*

Cite This: *J. Phys. Chem. C* 2024, 128, 7723−7732

Read Online

ACCESS | Metrics & More | Article Recommendations | Supporting Information

ABSTRACT: In focused ion-beam-induced deposition (FIBID) processes, the deposition rate and deposit composition are determined by the interplay between ion-induced deposition and sputtering of the deposited atoms. To provide independent insights into these two facets of FIBID, an ultrahigh vacuum (UHV) surface science approach employing in situ X-ray photoelectron spectroscopy (XPS) and mass spectrometry (MS) has been used to study how the identity of incident ions (Z = He, Ne, Ar, H_2 or D_2) influences ion-induced (i) deposition from adsorbed $Me_3PtCpMe$ and (ii) sputtering of the PtC_x films created from $Me_3PtCpMe$. For each of the ions studied, the initial decomposition/deposition step could be described as $Me_3PtCpMe_{(ads)} + Z_{(g)}^{+} \rightarrow PtC_{9-x(ads)} + xCH_{4(g)} + H_{2(g)}$ although the rate and extent of carbon loss from the $Me_3PtCpMe$ precursor depended on the ion identity, with heavier ions (Ar^+, Ne^+) leading to faster and more extensive fragmentation. For the heavier ions, these findings were ascribed to direct momentum/energy transfer between incident ions and adsorbed precursor molecules, while for the lighter ions, there is an increasing contribution from secondary electrons generated by ion−substrate interactions. While the Pt atom purity associated with ion-induced precursor decomposition was lower for the lighter ions, ion-induced sputtering of PtC_x films by lighter ions produced the greatest increase in metal content (i.e., purity), due to the extremely poor mass match with Pt. Indeed, sputtering of nanometer-thick PtC_x films by H_2^+/D_2^+ produced essentially pure Pt films, as measured by XPS. Increasing the substrate temperature during sputtering, however, inhibited the purification process. The results of these findings in the context of FIBID, conducted in the presence of a constant partial pressure of precursor molecules, are also discussed.

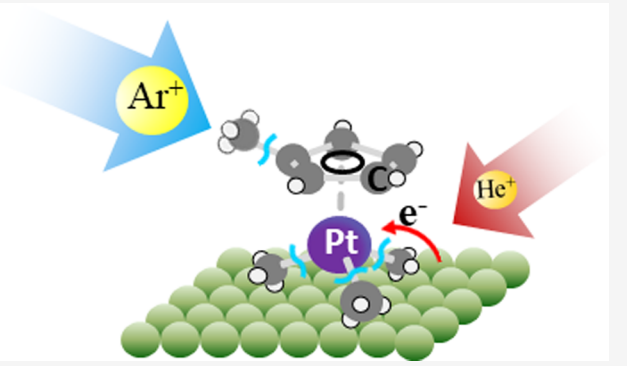

INTRODUCTION

Focused ion-beam-induced deposition (FIBID) of organometallic precursors is a charged particle, bottom-up technique capable of directly fabricating metal-containing nanostructures.[1−5] Some of the differences between FIBID and focused electron beam-induced deposition (FEBID) are that FIBID has higher current densities leading to more rapid deposition rates,[6] produces deposits with higher metal contents than FEBID, and has a wider choice of charged particle sources.[7−11] Differences in the microstructures of FIBID and FEBID materials have also been reported. For example, in a recent comparative FIBID/FEBID study using the metal silicide precursor $H_2Si(Co(CO)_4)_2$, it has been observed that the FIBID material is typically porous, while a measurably more dense deposit is obtained by FEBID.[12] FIBID also presents advantages over more traditional lithographic processes, such as electron beam lithography (EBL). Although EBL can create smaller, more precise features than FIBID, EBL typically requires the use of solvents and multistep processing, adding to manufacturing cost and complexity.[13,14] Compared to chemical vapor deposition (CVD) and atomic layer deposition (ALD), FIBID offers greater control over some aspects of the deposition process, e.g., spatial location, allowing for the formation of nanoscale patterns without the need for masks or sacrificial photoresist layers. In addition to the prototyping of nanostructures, the improved deposition control afforded by FIBID[15−17] has been exploited in various applications, such as circuit editing[18] and lithography mask repair.[19] Although ALD and CVD allow for greater throughput and conformal deposition, FIBID is an attractive alternative to these techniques.

In FIBID, metal-containing nanoscale materials are created through interactions between a focused ion beam and organometallic precursor molecules that are transiently adsorbed on the substrate surface. These ion-induced interactions can initiate a complex mixture of different

Received: January 29, 2024
Revised: April 15, 2024
Accepted: April 16, 2024
Published: April 30, 2024

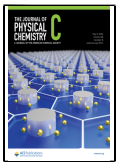

https://doi.org/10.1021/acs.jpcc.4c00630
J. Phys. Chem. C 2024, 128, 7723−7732

processes including secondary electron emission, surface atom sputtering, surface reconstruction, ion scattering, and ion implantation.[7,8,11,14,20−24]

The ultimate composition of a metal-containing deposit created by FIBID is a consequence of (i) the initial deposition process where reactions initiated by the ion beam cause the organometallic precursor to be converted into a nonvolatile deposit and (ii) postdeposition processing that occurs as a result of interactions between the deposited atoms and the ion beam.[13,14] Processes associated with the initial deposition step include secondary electron emission and energy transfer from the primary ion to the precursor (adsorbate). Ejected secondary electrons can be captured by the precursor leading to decomposition by either dissociative electron attachment or dissociative ionization, similar to the mechanisms present in focused electron beam-induced deposition (FEBID).[25] Alternatively, internuclear collisions between the ion and the adsorbate can also be responsible for deposition. Given these various possibilities, the composition of the material deposited from the precursor is likely to be sensitive to the mechanism(s) of deposition. Subsequent to deposition, inelastic and elastic collisions between ions and deposited atoms (i.e., postdeposition processing) can further alter the composition and thickness of the deposit as a consequence of sputtering.[6]

The effect of incident ion energy and ion flux becomes apparent when deposits made from $Me_3PtCpMe$ under different steady-state conditions are compared. Ga ion-induced deposition of Pt is considered the industry standard and is employed in many focused ion beam systems to prepare protective Pt films when extracting lamella for transmission electron microscopy (TEM) or etching material for cross-sectional scanning electron microscopy (SEM). However, the Pt film composition varies significantly during Ga^+-FIBID when the ion energy and/or the ion flux is altered.[26−32] For example, De Teresa et al. reported that when the Ga^+ ion energy is varied from 5 to 30 keV, the Pt content in nanodeposits decreases from 27 to 17%, while the C content remains >60% and the Ga content remains ≈10%.[26] In contrast, Puretz and Swanson reported that use of 25 keV Ga^+ resulted in Pt deposits with a composition of 37% Pt, 47% C, and 13% Ga.[28] Telari et al. maintained the Ga^+ ion energy at 30 keV while varying the ion flux. They observed that the Pt composition increased from 18 to 22% with increasing ion flux while the C content decreased from 72 to 69% and the Ga content slightly increased from 9 to 11%.[31] When the Ga^+ energy was increased to 32 keV, Tao et al. reported higher (46%) Pt contents with 24% C and 28% Ga.[30] This study also noted that the C content decreased with increasing ion current. In all of these previous FIBID examples, Pt structures were deposited from $Me_3PtCpMe$ under steady-state deposition conditions with the substrate at room temperature. However, FIBID has also been performed on cryogenically deposited $Me_3PtCpMe$ films; results from these studies revealed compositions of 12−13% Pt, 85% C, and 2% Ga, which are largely independent of beam energy in the range of 5−30 keV.[33] Overall, this analysis of the existing literature demonstrates how the film's composition is strongly dependent on the details of the deposition conditions, although it should be noted that some of these variations may well be a consequence of the inconsistency in the measurement techniques (e.g., incident energy variations in EDX) which confound many attempts for meaningful interlaboratory comparisons.

Previous studies have shown that the composition and structure of materials created by FIBID respond to the identity of the ion beam. Thus, at an incident energy of 8.5 keV and an ion flux of 7.0 pA, Rb^+-induced deposition generated Pt films with a composition of 25% C, 20% O, 49% Pt, and 5% Rb, whereas Ga^+-induced deposition under similar conditions (8.0 keV, 8.5 pA) resulted in Pt films with a composition of 22% C, 14% O, 37% Pt, and 27% Ga.[27] This also underscores the fact that in Ga^+ FIBID, the grown deposits often contain significant Ga contamination, affecting properties such as conductivity.[34] In Ar^+ FIBID, ion implantation becomes negligible as gaseous Ar escapes during deposition. However, the energy transfer between the ion and the adsorbate is still sufficient to affect sputtering of deposited atoms. Since the efficiency of energy transfer decreases as the ion mass decreases, He^+ FIBID can be used to reduce sputtering. Ion identity also impacts penetration depth and interaction volume.[23] Specifically, lighter ions (i.e., H^+, He^+) have lower cross sections for internuclear collisions resulting in a deep narrow interaction volume, whereas heavier ions (Ar^+, Ga^+) have greater internuclear collision cross sections resulting in a shallow broad interaction volume.[21,23] For lighter ions, an increased penetration depth and larger interaction volumes may result in larger deposits mediated by secondary electrons, as opposed to more localized deposits created by heavier ions that deposit most of their energy directly at the surface. Furthermore, ion identity has a well-established effect on differential sputtering of atoms from surfaces based on the role that mass matching plays in determining overall momentum/energy transfer efficiency.[35]

To probe the interactions between incident ions and adsorbed organometallic precursors, we employed *in situ* X-ray photoelectron spectroscopy (XPS) and mass spectrometry (MS). This ultrahigh vacuum (UHV) surface science approach involves studying ion-induced reactions of thin films of organometallic precursors physisorbed onto inert substrates. Information on the change in film composition and metal oxidation state can be acquired in situ as a function of ion dose, providing fundamental molecular-level insights into the charged particle-induced deposition mechanism.[7,8,11,25,36] In this way, it has previously been determined that the reaction cross section of Ar^+-induced deposition of $Me_3PtCpMe$ is 2 orders of magnitude greater than that of electron-induced deposition and occurs via momentum transfer from the incident ion to adsorbed precursor molecules. Moreover, the conversion of $Me_3PtCpMe$ into nonvolatile deposited atoms was accompanied by desorption of all four methyl groups.[7] By using relatively large Ar^+ beams (≈1 mm diameter) with Gaussian-shaped intensity distributions, we were also able to identify precursor and ion-limited regimes within a single deposit.

In this study, we employed this same UHV surface science approach to study how ion mass and identity affect the deposition and growth of Pt films created from $Me_3PtCpMe$. The notable advantage of the UHV surface science approach is that different facets of IBID can be examined in isolation, which is not possible when deposits are grown in the presence of a constant partial pressure of precursor molecules. Specifically, by using a variety of different ions (Ar^+, Ne^+, He^+, H_2^+, D_2^+), we explore the role that ion mass and identity play in determining (i) ion-induced deposition from $MeCpPtMe_3$ and (ii) sputtering of the PtC_x films formed by precursor deposition. To isolate the role of ion identity, the ion

https://doi.org/10.1021/acs.jpcc.4c00630
J. Phys. Chem. C 2024, 128, 7723−7732

energy was held constant (4 keV), and $Me_3PtCpMe$ was used as the common metal-containing precursor.

EXPERIMENTAL SECTION

General Description of Apparatus. Studies were conducted in a stainless steel UHV system as described elsewhere.[7] Argon (Airgas, 99.999%), deuterium (Sigma-Aldrich, 99.96 atom % D), helium (Airgas, 99.999%), hydrogen (Airgas, 99.999%), and neon (Cryogenic Rare Gas, 99.999%) were used without purification. The gas manifold was flushed with 20 psi of the desired gas and evacuated to <10 mTorr 3 times to prevent cross-contamination between gases. A separate gas line was installed for experiments involving deuterium (D_2). Gas purity in the vacuum chamber was verified by mass spectrometry (MS). Trimethyl-(methylcyclopentadienyl)platinum(IV) ($Me_3PtCpMe$, 99%) was purchased from Strem Chemicals and purified by several freeze−pump−thaw cycles until impurities such as H_2O and air (N_2 and O_2) were no longer detected by MS. A cooled, inert, 15 × 15 mm^2 tantalum/tantalum oxide substrate (200 ± 5 K) was exposed to $Me_3PtCpMe$ vapor to produce nanometer-scale thick films of precursor molecules, as determined by the attenuation of the substrate (Ta 4f, IMFP = 1.7 nm) signal in X-ray photoelectron spectroscopy (XPS) as shown in Figure S1 in the Supporting Information.[7,37,38] At this temperature, $Me_3PtCpMe$ adsorbs to the substrate surface where the precursor film can be subjected to ion beam irradiation without the risk of thermal degradation or desorption. Based on other studies, we have assumed that the Pt films formed by IBID of $Me_3PtCpMe$ in this study are homogeneous.[7,26−33]

XPS was performed with a PHI 5400 spectrometer using a Mg Kα X-ray source with an incident energy of 1253.6 eV, a pass energy of 22.38 eV, and a photoelectron takeoff angle of 57°. Photoelectron spectra were processed using CasaXPS, a commercially available analysis software package.

Mass spectrometry was performed with a Balzers Prisma QMA 200 mass spectrometer. A PHI 04−303 differentially pumped ion gun served as the source for ion irradiation during experiments and Ar^+ sputter cleaning between experiments. The spot size produced by this ion source was determined to be 1 mm by measuring the diameter of an exposed phosphor target as well as by previous SEM analysis of steady-state deposits on Si substrates.[7] Ion beam exposure was conducted by rastering the ion beam over a 1.0 × 1.0 cm^2 area.

Ion Irradiation of $Me_3PtCpMe$ Thin Films. The ion irradiation of $Me_3PtCpMe$ thin films is described in Scheme 1. Pt reduction studies were conducted on thin 1−2 nm precursor films produced by exposing the cooled (200 K) substrate to 150 Langmuir (1.0 × 10^{-6} Torr × 2.5 min) of $Me_3PtCpMe$ vapor. These films were subsequently exposed to a 4.02 keV ion beam. A bias voltage of +20 V was applied to the sample to attract ejected secondary electrons and thereby ensure an accurate target current measurement. Thus, the net ion beam energy was 4.0 keV. Exposure of precursor films to H_2^+, D_2^+, and He^+ was conducted at 4.0 keV and a target current of 70 nA, corresponding to an ion flux of 4.4 × 10^{11} ions/s. In separate control experiments, we determined that at this ion flux, the extent of $Me_3PtCpMe$ decomposition from X-ray-induced secondary electron emission during acquisition of XPS data is negligible compared to the effects of the ion-induced process. For Ne^+ and Ar^+, irradiation was conducted at a net energy of 4.0 keV and a lower target current of 20 nA (1.2 × 10^{11} ions/s). This lower target current was necessary to slow the rate of $Me_3PtCpMe$ decomposition for these heavier ions so that XPS data could be used to quantify the deposition rate.

Scheme 1. Deposition of Thin $Me_3PtCpMe$ Films and Their Subsequent Ion-Beam-Induced Deposition/Decomposition Using Different Ions (Z = Ar, Ne, D_2, He, H_2)

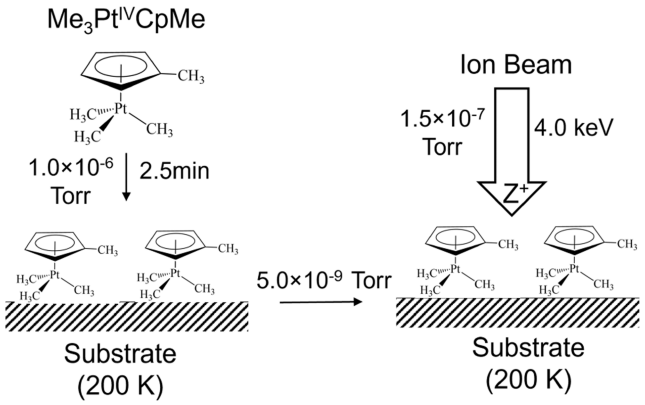

Ion Irradiation of PtC_x Films. To probe the effects of ion bombardment on PtC_x films generated from $Me_3PtCpMe$, thicker (≥4 nm) multilayer $Me_3PtCpMe$ films were produced by exposing a cooled (200 K) substrate to 6000 Langmuir (5.0 × 10^{-6} Torr × 1200 s) of $Me_3PtCpMe$ vapor. These films were then exposed to a 500 eV electron beam (20 μA, 30 min) to produce a nonvolatile PtC_x film. A Specs FG 15/40 flood gun was used as the electron source. The flood gun was used at an energy of 480 eV with a sample bias of +20 V to produce an incident electron energy of 500 eV. The target current was maintained at 20 μA during electron irradiation.

This process of deposition and e-beam irradiation was repeated following three consecutive doses of $Me_3PtCpMe$, ensuring that films were sufficiently thick to monitor changes in the composition and thickness of the film as a result of subsequent ion irradiation (i.e., sputtering). Following the third deposition/irradiation, the substrate was allowed to warm to ambient temperature (307 K) overnight. PtC_x films were subsequently irradiated at ambient temperature (307 K) with different ions at an energy of 4.0 keV and a target current of 5.0 μA, corresponding to an ion flux of 3.1 × 10^{13} ions/s. These parameters remained constant for all five ion beams. The PtC_x film growth and sputtering procedure is illustrated in Scheme 2.

To probe the thermal effects on the interactions between H_2^+ and PtC_x films, the substrate temperature was maintained at a constant value (210, 310, 410, and 510 K) during ion irradiation using a PID controlled 0−4 V, 0−30 A DC power supply (Eurotherm 2408 PID controller, Sorenson DCR 20−25B PSU). In these temperature-dependent studies, the H_2^+ ion beam was maintained at an energy of 4.0 keV and a target current of 18.0 μA, corresponding to an ion flux of 1.1 × 10^{14} ions/s.

RESULTS AND DISCUSSION

Ion-Induced Decomposition of $Me_3PtCpMe$. In IBID, the initial step in the growth of a Pt-containing structure is decomposition of the transiently adsorbed precursor molecule into a nonvolatile product that forms the building block of the deposit. In this part of the study, we used *in situ* XPS to explore

https://doi.org/10.1021/acs.jpcc.4c00630
J. Phys. Chem. C 2024, 128, 7723−7732

Scheme 2. Deposition of Thick Films for Ion Sputtering Studies[a]

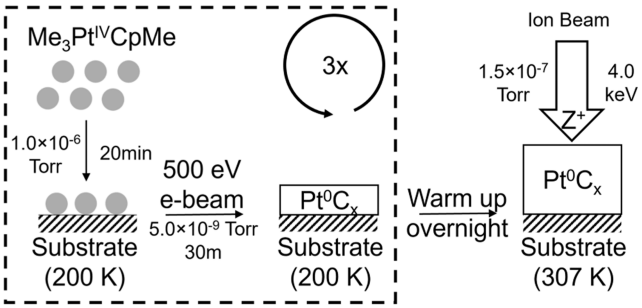

[a]Three cycles of precursor and e^- beam exposure (dashed box) were conducted to create a PtC_x film. Ion irradiation was conducted on the PtC_x film after it had reached room temperature.

how reactions between adsorbed $Me_3PtCpMe$ precursor molecules and incident ions are influenced by the ion identity. Experimentally, these studies were performed on 1−2 nm thick films of precursor molecules adsorbed onto a TaO_x substrate at low temperatures as shown in Scheme 1.

Pt Reduction Kinetics. The X-ray photoelectron spectra in Figure 1 display Pt 4f transitions of an adsorbed $MeCpPtMe_3$ thin film at 200 K as a function of increasing ion dose (bottom to top) for H_2^+(left) and Ne^+(right). The corresponding Pt 4f transitions for $Me_3PtCpMe$ thin films irradiated with D_2^+, He^+, and Ar^+ are presented in Figure S2 in the Supporting Information. In the absence of ion exposure, $Me_3PtCpMe$ adsorbs molecularly and the Pt $4f_{5/2}$ and Pt $4f_{7/2}$ doublet at 76.9 and 73.5 eV, respectively, is attributed to Pt(IV) from the $Me_3PtCpMe$ precursor (blue curves in Figure 1).[7,36,39] As a result of ion exposure, a new Pt 4f doublet (red curves) appears with values shifted toward a lower binding energy (1.9 eV) as compared to the peaks associated with the precursor. This shift has been interpreted previously to indicate Pt reduction from the Pt(IV) of $Me_3PtCpMe$ to a Pt(0) species embedded in a carbonaceous matrix.[7,36] Comparing the transformations to the Pt 4f regions observed when Ne and H_2 are used as source gases in Figure 1 demonstrates that this reduction occurs regardless of the ion identity. Indeed, this Pt reduction process has been observed in previous studies of $MeCpPtMe_3$ films exposed to charged (electron[36] and Ar^+ ion[7]) particles. However, the ion mass affects the reaction kinetics, as reflected by the required ion dose to complete the reduction. Thus, for H_2^+ (4.0 keV, 70 nA) and Ne^+ (4.0 keV, 20 nA), the ion dose required to effect complete Pt reduction is 252 and 42 $\mu C/cm^2$, respectively. For each ion, the total reaction cross section for Pt reduction can be determined from the best fit values obtained from a first-order kinetic analysis of the ion-induced Pt(IV)−Pt(0) conversion. From the kinetic decay curves shown in the bottom plot in Figure 1, H_2^+, D_2^+, and He^+ have similar reaction cross sections at $\approx 3.2 \times 10^{-15}$ cm^2, whereas Ne^+ and Ar^+ have significantly higher reaction cross sections at $\approx 2.1 \times 10^{-14}$ cm^2.

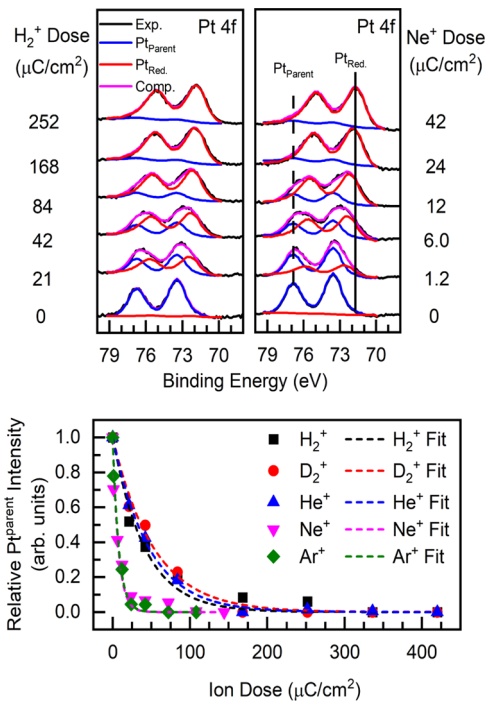

Figure 1. (Top) X-ray photoelectron spectra in the Pt 4f region of adsorbed $Me_3PtCpMe$ thin films exposed to different ion doses of (left) H_2^+ and (right) Ne^+ ions, both at 4.0 keV. The resultant spectra have been deconvoluted into contributions from two species; the parent Pt^{parent} doublet (blue) and a product $Pt^{(red.)}$ doublet (red). The magenta trace is the composite of the $Pt^{(IV)}$ and $Pt^{(red.)}$ traces. (Bottom) Kinetics of $Me_3PtCpMe$ reduction for each of the ions studied in this investigation based on the rate of decrease in the precursor (Pt^{parent}) coverage as a result of 4.0 keV ion bombardment; the dashed lines represent the best fit analysis based on a first-order kinetic process.

In addition to the reaction rate, ion mass also influences the change in film composition as expressed by the C/Pt ratio that accompanies the ion-induced decomposition of $Me_3PtCpMe$. Thus, Figure 2 (top left) presents the change in the C/Pt ratio for $Me_3PtCpMe$ films during the Pt(IV) reduction process for each of the five ions studied in this investigation. Prior to ion irradiation, the C/Pt ratio is 9:1, reflecting the stoichiometry of the $Me_3PtCpMe$ precursor. Upon ion exposure, this ratio decreases for all ions, although the magnitude of the C/Pt ratio decrease is sensitive to the ion identity. Specifically, the extent to which the C/Pt ratio decreases increases with increasing ion mass. Thus, exposure to Ne^+ and Ar^+ results in Pt films with C/Pt ratios of 6.2 and 5.7 at ion doses sufficient to completely reduce the $Me_3PtCpMe$. These ratios are measurably lower than the C/Pt ratios observed when $Me_3PtCpMe$ is fully decomposed by irradiation with the lighter ions, which range from 7.5 to 8.0.

This decrease in Pt purity (i.e., higher C/Pt ratios) for the lighter ions is displayed spectroscopically in the top right panel of Figure 2 where the normalized C 1s peak profiles are shown for each ion. In each case, the ion dose is just sufficient to have effected complete reduction of the Pt(IV) species, corresponding to complete decomposition of the $Me_3PtCpMe$ precursor. The bottom left panel in Figure 2 demonstrates that during ion irradiation, the extent of Pt(IV) reduction is directly correlated with the change in the film's overall C/Pt ratio, while the absolute decrease in the C/Pt ratio is ion-dependent. The bottom right panel reveals that the binding energy of the reduced Pt species formed by ion irradiation is invariant to the ion identity.

For each ion, a comparison of the reaction cross section determined from Figure 1 along with the final C/Pt ratio determined from Figure 2 is listed in Table 1. As the ion mass increases from H_2^+ to Ar^+, the reaction cross section for

https://doi.org/10.1021/acs.jpcc.4c00630
J. Phys. Chem. C 2024, 128, 7723−7732

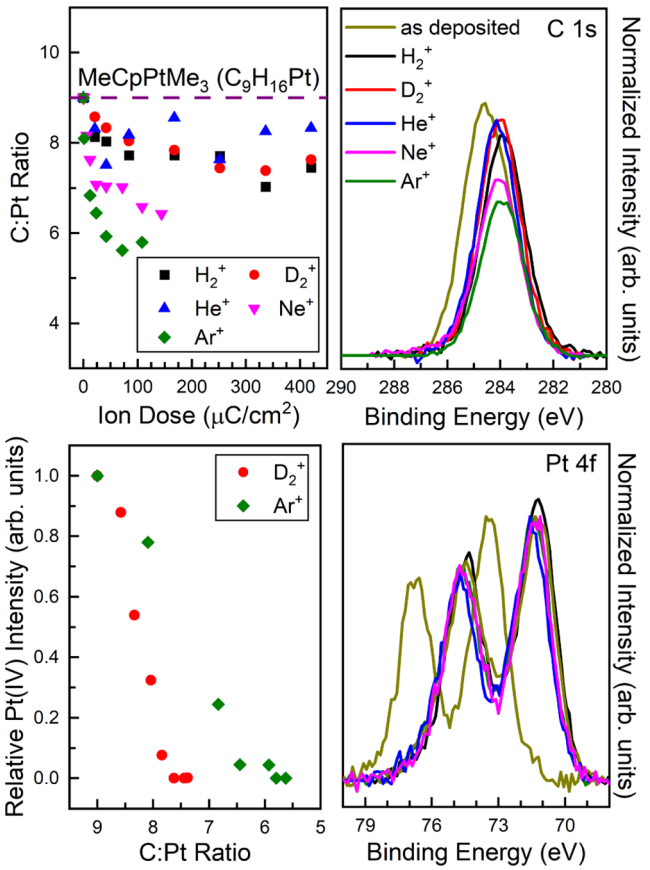

Figure 2. (Top left) Comparison of the change in C/Pt ratio that occurs for $Me_3PtCpMe$ films exposed to different ions, plotted as a function of ion dose. The dashed purple line represents the initial precursor stoichiometry (9:1). (Bottom left) Correlation between Pt reduction and the change in C/Pt ratio in $Me_3PtCpMe$ films exposed to D_2^+(red circles) and Ar^+(green triangles). (Top right) Photoelectron spectra of the C 1s (top right) and Pt 4f (bottom right) regions after complete $Me_3PtCpMe$ reduction with different ions. For each of the XPS spectra, intensities are normalized to the initial C/Pt ratio of 9:1 in the "as deposited" $Me_3PtCpMe$ film.

$Me_3PtCpMe$ increases, while the C/Pt ratio associated with the decomposition product decreases.

Table 1. Reaction Cross Sections for $MeCpPtMe_3$ Decomposition and C/Pt Product Ratios for Charged Particle Reactions with $MeCpPtMe_3$

Particle	σ ($\times 10^{15}$ cm^2)	C/Pt ratio
e^-	0.137[a]	8.0[a]
H_2^+	3.8 ± 0.3	7.5
D_2^+	3.0 ± 0.2	7.5
He^+	3.4 ± 0.1	8.0
Ne^+	22 ± 3	6.2
Ar^+	21 ± 3	5.7

[a]Wnuk et al.[36]

For all of the ions studied (Z = He, Ne, Ar, H_2 or D_2), MS revealed the desorption of CH_4 and H_2 during ion irradiation as shown in Figure 3 for Ar and D_2. This observation is consistent with the ion-induced decomposition of $Me_3PtCpMe$ by the following mechanism[7]

$$Me_3PtCpMe(ads) + Z^+ \rightarrow PtC_{9-x}(ads) + xCH_4(g) + H_2(g)$$

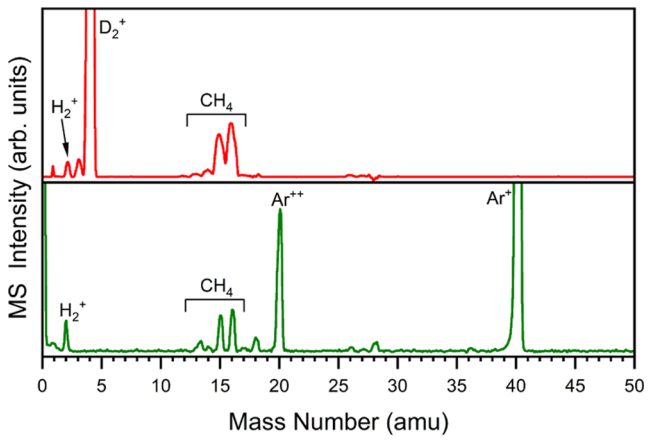

Figure 3. Mass spectra of the neutral desorption products observed during the ion-beam irradiation of $Me_3PtCpMe$ by (top) D_2 and (bottom) Ar.

It should be noted that this mechanism is not charge-balanced, as any charge buildup is neutralized by having the substrate electrically grounded. For Ar^+ irradiation, the experimentally observed decrease in C/Pt ratio has been attributed to the loss of all four methyl carbon atoms while all of the carbon atoms associated with the cyclopentadienyl ring are retained.[7] This process was attributed to direct momentum/energy transfer from the incident ion to the film of adsorbed $Me_3PtCpMe$ molecules, providing enough energy to cleave all three of the Pt−CH_3 bonds and the Cp−CH_3 bond. We attribute the dominance of direct ion−adsorbate interactions in the case of Ar^+ irradiation to a consequence of the relatively large size of the ion and the correspondingly small (≪1 nm) inelastic mean free path.[21,35,40]

The sensitivity of both the reaction rate and change in C/Pt ratio described in Figures 1 and 2 and Table 1 indicate that the ion-induced deposition mechanism is, however, sensitive to the ion identity/mass. In principle, this change could be a result of less efficient momentum-energy transfer due to the poorer mass match between lighter ions and adsorbed $Me_3PtCpMe$ molecules. However, even for the lightest ion (H_2^+), a simple kinematic model indicates that the maximum energy transfer would still be ≈100 eV. This is still well in excess of the ≈7 eV needed to cleave all three of the Pt−CH_3 bonds and the Cp−CH_3 bond as seen for Ar^+, inconsistent with our experimental observations. Moreover, if kinematic energy transfer was dominant for all of the ions, then we would expect similar rates of Pt(IV) reduction, which is not the case (Figure 1).

We interpret our ion-dependent experimental observations to indicate that for the lighter ions (He^+, H_2^+, and D_2^+) the $Me_3PtCpMe$ decomposition mechanism also involves reactions between adsorbed $Me_3PtCpMe$ and secondary electrons generated by interactions of the primary ions with the substrate. Support for this idea comes from the inelastic mean free path of these lighter ions being similar (≈1 nm) to the thickness of the films. This will lead to an increased role for ion−substrate interactions, producing a large number of low-energy secondary electrons capable of decomposing $Me_3PtCpMe$ by means of dissociative electron attachment

https://doi.org/10.1021/acs.jpcc.4c00630
J. Phys. Chem. C 2024, 128, 7723−7732

(DEA).[14,25] This DEA process involves the formation of a transient negative anion and the desorption of one CH_3 group, leading to a C/Pt ratio of 8:1.[25] For $H_2^+/D_2^+/He^+$, the increased role of secondary electrons in promoting precursor decomposition is supported experimentally not only by a change in reaction rate but also by the change in C/Pt ratio being similar to the change observed during electron beam-induced $Me_3PtCpMe$ dissociation.[36] For the intermediate-sized Ne^+ ions, the experimental data suggests that ion–$Me_3PtCpMe$ interactions leading to decomposition are dominated by kinematic energy transfer but with some contribution from secondary electrons. Thus, particle size plays a role in precursor decomposition where the smaller particles (e^- and He^+) have a greater penetration volume[21] into the substrate than the larger particles. This causes more inelastic collisions with the substrate, leading to a greater contribution of secondary electrons, which can be captured by the adsorbate to induce dissociation. Since the only process that accompanies ion-beam-induced deposition is the ejection of methane, changes in the film's thicknesses that accompany ion beam irradiation are not particularly diagnostic because the vast majority of the atoms remain. However, the largest decrease in the thickness of $Me_3PtCpMe$ films was observed during exposure to the heavier ions (Ar^+ and Ne^+), consistent with a greater loss of carbon during deposition.

It should be noted, however, that in principle, the influence of ion identity on reaction rates and extent of reaction could also reflect changes to the nature of ion/$Me_3PtCpMe$ interactions. Thus, Indrajith et al. determined that the decomposition of gaseous $Fe(CO)_5$ occurs by electronic excitation and electron capture when exposed to $^4He^+$, whereas the dominant decomposition pathway is nuclear excitation by elastic collisions between the ions and the Fe, C, and O atoms in the precursor when exposed to the heavier ions (e.g., $^{20}Ne^+$, $^{40}Ar^+$).[24] If this same sensitivity to ion mass is operative in the present study, it would produce the trend that we observe experimentally, with a lower degree of carbon loss for lighter ions.

Ion-Induced Sputtering of Deposited PtC_x Films. To examine the effect of ion identity on deposits created by the decomposition of $Me_3PtCpMe$, PtC_x films (≥4 nm thickness) were first prepared by exposing $Me_3PtCpMe$ multilayers to the effects of electron irradiation. This enabled the creation of deposits with a nominal C/Pt ratio of ≈8:1 based on the known effects of electron irradiation.[36] Films of consistent initial composition and similar thicknesses could therefore be created and subsequently exposed to different ions by using XPS to quantify both changes in film composition and film thickness.

The photoelectron spectra in Figure 4 for $t = 0$ correspond to the C 1s and Pt 4f transitions of the PtC_x film prior to H_2^+ and Ne^+ ion irradiation. The Pt peak positions (74.6 and 71.3 eV) are consistent with the reduced Pt(0) species produced upon precursor ($Me_3PtCpMe$) decomposition,[7,36] while the absence of any substrate signal in the Ta 4f region indicates that the films are thicker than 4 nm. With the onset of H_2^+ and Ne^+ irradiation, the intensity of the C 1s peak steadily decreases until it is no longer observable. However, this process is markedly more efficient for Ne^+ compared to H_2^+. Thus, carbon removal is completed with 90 and 1152 mC/cm^2 doses of Ne^+ and H_2^+, respectively. As carbon is removed from the film by H_2^+, the intensity of the Pt signal increases. Indeed, at a H_2^+ exposure of 1152 mC/cm^2, the XPS spectrum consists

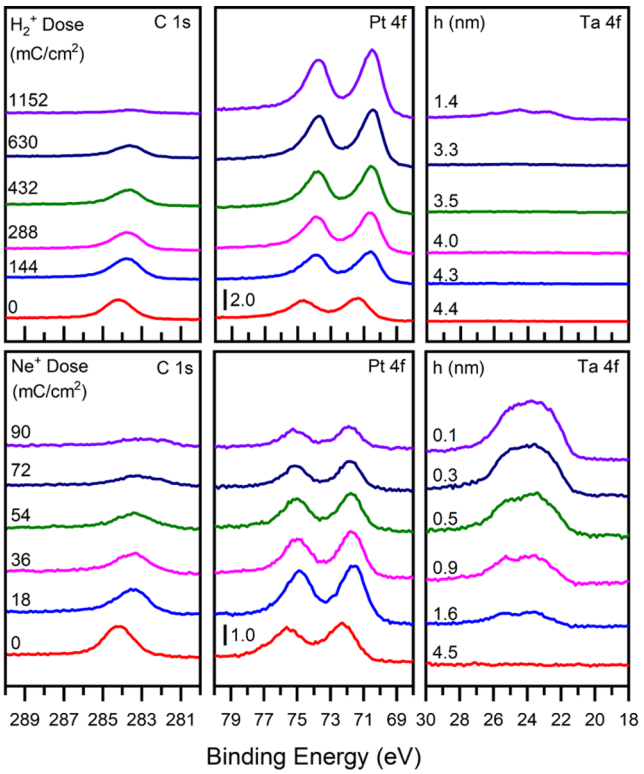

Figure 4. X-ray photoelectron spectra of adsorbed $Me_3PtCpMe$ thick films on a Ta/TaO_x substrate irradiated with (top) H_2^+ and (bottom) Ne^+ at the indicated ion doses with a constant energy of 4.0 keV; h represents the thickness of the adsorbed layer.

exclusively of the Pt 4f doublet without any C 1s signal. For Ne^+, initial carbon removal is also accompanied by an increase in Pt signal intensity, but for ion doses >18 mC/cm^2, the Pt 4f signal decreases and is accompanied by a marked increase in the Ta 4f substrate signal. Thus, for a Ne^+ dose of 36 mC/cm^2, the film thickness is <1 nm, and by 90 mC/cm^2, the film has been completely removed (film thickness 0.1 nm). In contrast, no discernible substrate signal is observed during H_2^+ until an ion dose of 1152 mC/cm^2. A scaled version of the Ta 4f transition as a function of H_2^+ dose is presented in Figure S3 in the Supporting Information. The slight changes in the substrate signal are sufficient to calculate the film thickness, as presented in Figure 4.

For each of the five ions studied, the changes in film composition and thickness (sputter efficiency) are presented in Figure 5 as a function of the ion dose. The left panel of Figure 5 highlights the marked increase in the sputter rate that occurs as the ion mass increases. Thus, a film thickness of ≈2 nm is reached after ion doses of <50 mC/cm^2 for Ar^+ and Ne^+, 300–450 mC/cm^2 for He^+ and D_2^+, and ≈900 mC/cm^2 for H_2^+. This dependence is attributed to the relationship between the ion mass and the penetration depth and interaction volume of the ion beam with the deposited PtC_x films. Heavier particles such as Ar^+ and Ne^+ have broad, shallow interaction volumes within films.[21] This leads to a greater probability of momentum/energy transfer at the surface and an increased likelihood of physical sputtering. Conversely, He^+ and H_2^+ have narrow deep interaction volumes within films[21] and a correspondingly greater probability of momentum/energy transfer within the bulk and less surface sputtering.

https://doi.org/10.1021/acs.jpcc.4c00630
J. Phys. Chem. C 2024, 128, 7723–7732

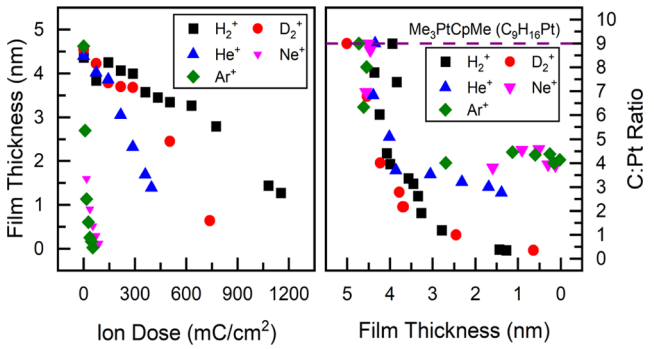

Figure 5. (Left) Change in the film thickness as a result of 4.0 keV ion bombardment. (Right) Change in the Pt purity (C/Pt ratio) as the PtC_x film is sputtered. The dashed line indicates the C/Pt ratio observed for the initial $Me_3PtCpMe$ film.

The right-hand panel of Figure 5 describes the relationship between the film composition, expressed as the C/Pt ratio, and the film thickness. For all of the ions the C/Pt ratio decreases upon irradiation. This decrease in C/Pt observed upon ion irradiation is an indication of preferential carbon sputtering. This reflects the poor mass match between any of the incident ions (amu ranging from 4 to 40) and Pt (195 amu) as compared to C (12 amu) which leads to greater efficiency of ion energy transfer to surface-bound C atoms. However, high-purity Pt films (here considered to be C/Pt $\leq$ 1) are achieved only for H_2^+ and D_2^+. This reflects the increasingly poor mass matching between these lighter ions and Pt in particular, which results in Pt having a dramatically lower sputter rate than C when it is exposed to H_2^+ and D_2^+ such that Pt sputtering is not measurable in these thin film studies. This explains why films with the highest Pt content are produced when the PtC_x films are irradiated with lighter ions. Interestingly, for D_2 ($^2H_2$, 4 amu), the film purity trend follows the same trend as $^1H_2$ (2 amu) rather than ^4He, albeit with an increased rate of sputtering for D_2^+ vs H_2^+. This suggests that there may be an additional contribution to the improved Pt purity that arises from chemical sputtering, caused by the hydrogen and deuterium atoms/ions liberated by H_2^+/D_2^+ dissociation during ion irradiation.[41−45] In terms of creating high-purity Pt films, H_2^+ is preferred over D_2^+ because it allows for comparable purification but at a reduced sputtering rate.

Implications for IBID. Structures are created by IBID in a constant partial pressure of precursor molecules where all of the elementary reaction steps are occurring simultaneously.[14,18,46−48] Thus, adsorbed $Me_3PtCpMe$ molecules are undergoing decomposition into nonvolatile species, while deposited atoms at the growth surface are simultaneously being subjected to the effects of ion bombardment. In contrast, the UHV surface science approach allows us to independently study two of these elementary steps; (i) ion−adsorbate interactions that contribute to the conversion of volatile precursor molecules into nonvolatile deposited atoms and (ii) subsequent postdeposition processing that occurs in the form of sputtering. Figures 1 and 2 and Table 1 indicate that initial deposition and purification of $Me_3PtCpMe$ by means of ion−adsorbate interactions are more efficient for heavier ions (e.g., Ar^+). In this respect, it is important to note that our UHV experiments are most representative of those that would be encountered in an ion-limited deposition. Indeed, in related IBID experiments, we have observed that thicker deposits are created from $Me_3PtCpMe$ when Ar^+ is used as the source gas compared to He^+ or H_2^+, consistent with the idea that the use of heavier ions leads to higher reaction/deposition rates. However, in many IBID experiments, the growth surface will not be fully covered by a monolayer of precursor molecules, and as a result, other processes can also contribute to precursor decomposition/deposition. These include reactions between sputtered substrate atoms and/or secondary electrons with gas phase precursor molecules.[7,11,14,34,35] Regardless of the detailed mechanisms, any benefits afforded by using heavier ions in the initial deposition step (Figures 1 and 2) are offset by significantly higher sputtering rates and less efficient Pt purification during sputtering as compared to lighter ions (e.g., He^+), as shown in Figures 4 and 5. Thus, our results suggest that IBID using lighter ions holds the greater promise for creating high-purity Pt deposits from $Me_3PtCpMe$ because of the >20-fold decrease in sputter rate and the significant decrease in carbon content that accompanies sputtering. However, to take advantage of these benefits, it will be necessary to conduct IBID under precursor-limited deposition conditions, where deposited atoms are subject to extensive ion bombardment at the growth surface before they become incorporated into the interior of the deposit.

Impact of Substrate Temperature. Motivated by the success of creating nearly pure Pt deposits from PtC_x films using H_2^+, we explored the impact of substrate temperature on H_2^+ purification. Analysis of the C 1s and Pt 4f XP spectra in Figure 6 indicates that the rate of carbon removal and the corresponding increase in Pt 4f signal decreased as the substrate temperature increased from 210−510 K, highlighting that Pt purification is highest at lower substrate temperatures. This is also shown in the bottom right panel of Figure 6, where the changes in C/Pt ratio are plotted as a function of ion dose for substrate temperatures ranging from 210−510 K. The top right panel in Figure 6 compares the corresponding sputtering

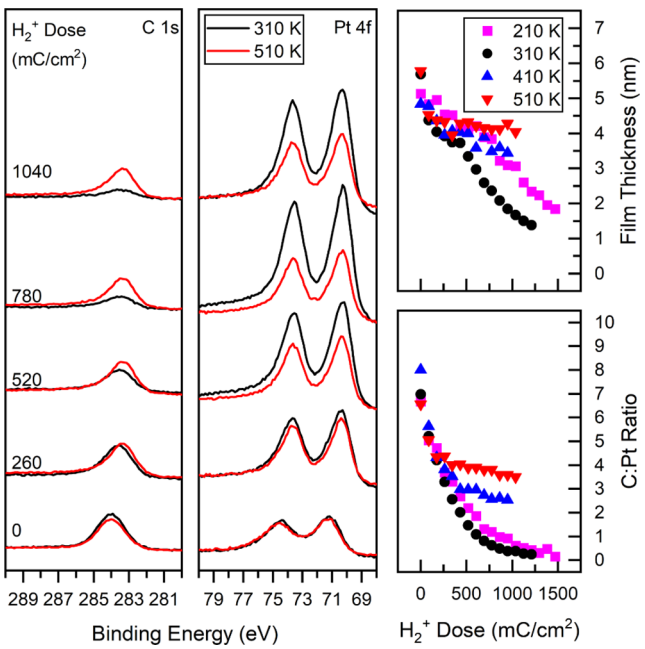

Figure 6. Changes in the (left) C 1s and (middle) Pt 4f XP spectra of $Me_3PtCpMe$ films maintained at temperatures of 310 K (black) and 510 K (red) as a result of 4.0 keV H_2^+ bombardment. (Right) Dependence of H_2^+-induced film (top) sputtering and (bottom) purification on substrate temperature.

https://doi.org/10.1021/acs.jpcc.4c00630
J. Phys. Chem. C 2024, 128, 7723−7732

efficiencies at different substrate temperatures, by measuring the change in film thickness as a function of ion dose. This data demonstrates that the sputtering efficiency increases slightly at lower substrate temperatures in line with the general observation that physical sputtering does not demonstrate a strong dependence on substrate temperature.[49,50]

Several possibilities exist for the temperature dependence on purification observed in this study. One possibility is that the film may undergo structural/morphological transformations at higher temperatures. Support for this idea comes from previous studies which have shown significant changes in this temperature region for Pt/C films deposited by EBID.[51] These changes include increases in Pt particle size with the possibility of changes in the hybridization of carbon due to thermal hydrogen evolution. Any of these structural changes could modify the efficiency of carbon atom sputtering since physical sputtering is known to be sensitive to the form and phase of carbon.[52]

Another possibility is that the substrate temperature dependence is a reflection that carbon removal by D_2^+ and H_2^+ is, in part, facilitated by Pt-catalyzed hydrogenation of amorphous carbon. The rate of this reaction would be critically dependent on the steady-state surface coverage of adsorbed hydrogen atoms formed during H_2^+ dissociation on Pt atoms. Temperature-programmed desorption studies indicate that H_2 desorption from Pt occurs at temperatures above 373 K[42−45] which would limit the availability of adsorbed hydrogen to react with and purify the PtC_x film at higher substrate temperatures.

CONCLUSIONS

In this study, we investigated the role of ion identity on (i) the ion-induced decomposition of adsorbed $Me_3PtCpMe$ and (ii) sputtering of PtC_x films deposited by precursor decomposition. When adsorbed $Me_3PtCpMe$ molecules are exposed to heavier ions (Ne^+ and Ar^+), precursor decomposition is driven by energy transfer that occurs during ion−adsorbate collisions, leading to higher reaction cross sections and a greater loss of carbon. For lighter ions (H_2^+, D_2^+, and He^+), changes in the film's composition and reaction cross section suggest that the process also contains a contribution from secondary electrons generated by interactions of the ion beam with the substrate. However, while heavier ions produce a greater increase in the Pt atom content during the initial deposition/decomposition step, the greatest increase in Pt purity during the subsequent sputtering of deposited PtC_x films occurs for H_2^+ and D_2^+. This is a consequence of the extremely poor mass match between these lighter ions and Pt, leading to very inefficient Pt atom sputtering as compared to C. Consequently, almost pure Pt films can be produced when nanometer-thick PtC_x films are sputtered by H_2^+ and D_2^+, although this purification process was less efficient at higher substrate temperatures. In the context of FIBID, our results suggest that films with the greatest Pt atom purity will be formed from $Me_3PtCpMe$ at lower substrate temperatures under precursor-limited deposition conditions using H_2^+.

ASSOCIATED CONTENT

Supporting Information

The Supporting Information is available free of charge at https://pubs.acs.org/doi/10.1021/acs.jpcc.4c00630.

Photoelectron spectra of the substrate (Ta 4f) for film thickness determination; changes in Pt 4f transition as a function of ion dose; and the Ta 4f spectra for thick PtC_x films as a function of H_2^+ irradiation (PDF)

AUTHOR INFORMATION

Corresponding Author

D. Howard Fairbrother − *Department of Chemistry, Johns Hopkins University, Baltimore, Maryland 21218, United States;* orcid.org/0000-0003-4405-9728; Email: howardf@jhu.edu

Authors

Mohammed K. Abdel-Rahman − *Department of Chemistry, Johns Hopkins University, Baltimore, Maryland 21218, United States;* orcid.org/0000-0002-8028-5258

Patrick M. Eckhert − *Department of Chemistry, Johns Hopkins University, Baltimore, Maryland 21218, United States;* orcid.org/0000-0001-6520-1821

Lisa McElwee-White − *Department of Chemistry, University of Florida, Gainesville, Florida 32611-7200, United States;* orcid.org/0000-0001-5791-5146

Complete contact information is available at: https://pubs.acs.org/10.1021/acs.jpcc.4c00630

Notes

The authors declare no competing financial interest.

ACKNOWLEDGMENTS

D.H.F. and L.M.W. thank the National Science Foundation for supporting this work through Grants CHE-1904559 and CHE-1904802.

REFERENCES

(1) Allen, F. I. A Review of Defect Engineering, Ion Implantation, and Nanofabrication Using The Helium Ion Microscope. *Beilstein J. Nanotechnol.* **2021**, *12*, 633−664.

(2) Jesse, S.; Borisevich, A. Y.; Fowlkes, J. D.; Lupini, A. R.; Rack, P. D.; Unocic, R. R.; Sumpter, B. G.; Kalinin, S. V.; Belianinov, A.; Ovchinnikova, O. S. Directing Matter: Toward Atomic-Scale 3D Nanofabrication. *ACS Nano* **2016**, *10*, 5600−5618.

(3) Tseng, A. A. Recent Developments in Nanofabrication Using Focused Ion Beams. *Small* **2005**, *1*, 924−939.

(4) Yu, J. C.; Abdel-Rahman, M. K.; Fairbrother, D. H.; McElwee-White, L. Charged Particle-Induced Surface Reactions of Organometallic Complexes as a Guide to Precursor Design for Electron- and Ion-Induced Deposition of Nanostructures. *ACS Appl. Mater. Interfaces* **2021**, *13*, 48333−48348.

(5) Höflich, K.; Hobler, G.; Allen, F. I.; Wirtz, T.; Rius, G.; McElwee-White, L.; Krasheninnikov, A. V.; Schmidt, M.; Utke, I.; Klingner, N.; et al. Roadmap for Focused Ion Beam Technologies. *Appl. Phys. Rev.* **2023**, *10*, No. 041311.

(6) Kim, C.-S.; Ahn, S.-H.; Jang, D.-Y. Review: Developments in Micro/Nanoscale Fabrication by Focused Ion Beams. *Vacuum* **2012**, *86*, 1014−1035.

(7) Abdel-Rahman, M. K.; Eckhert, P. M.; Fairbrother, D. H. Ion-Induced Surface Reactions and Deposition of Trimethyl-(methylcyclopentadienyl)platinum(IV). *J. Phys. Chem. C* **2022**, *126*, 15724−15735.

(8) Bilgilisoy, E.; Thorman, R. M.; Barclay, M. S.; Marbach, H.; Fairbrother, D. H. Low Energy Electron- and Ion-Induced Surface Reactions of $Fe(CO)_5$ Thin Films. *J. Phys. Chem. C* **2021**, *125*, 17749−17760.

(9) Bilgilisoy, E.; Thorman, R. M.; Yu, J.-C.; Dunn, T. B.; Marbach, H.; McElwee-White, L.; Fairbrother, D. H. Surface Reactions of Low-

Energy Argon Ions with Organometallic Precursors. *J. Phys. Chem. C* **2020**, *124*, 24795−24808.
(10) Thorman, R. M.; Jensen, P. A.; Yu, J.-C.; Matsuda, S. J.; McElwee-White, L.; Ingólfsson, O.; Fairbrother, D. H. Electron-Induced Reactions of $Ru(CO)_4I_2$: Gas Phase, Surface, and Electron Beam-Induced Deposition. *J. Phys. Chem. C* **2020**, *124*, 10593−10604.
(11) Thorman, R. M.; Matsuda, S. J.; McElwee-White, L.; Fairbrother, D. H. Identifying and Rationalizing the Differing Surface Reactions of Low-Energy Electrons and Ions with an Organometallic Precursor. *J. Phys. Chem. Lett.* **2020**, *11*, 2006−2013.
(12) Jungwirth, F.; Porrati, F.; Knez, D.; Sistani, M.; Plank, H.; Huth, M.; Barth, S. Focused Ion Beam vs Focused Electron Beam Deposition of Cobalt Silicide Nanostructures Using Single-Source Precursors: Implications for Nanoelectronic Gates, Interconnects, and Spintronics. *ACS Appl. Nano Mater.* **2022**, *5*, 14759−14770.
(13) Melngailis, J. Focused Ion Beam Technology and Applications. *J. Vac. Sci. Technol., B: Microelectron. Process. Phenom.* **1987**, *5*, 469−495.
(14) Utke, I.; Hoffmann, P.; Melngailis, J. Gas-Assisted Focused Electron Beam and Ion Beam Processing and Fabrication. *J. Vac. Sci. Technol., B: Microelectron. Nanometer Struct. Process., Meas., Phenom.* **2008**, *26*, 1197−1276, DOI: 10.1116/1.2955728.
(15) Keskinbora, K.; Grevent, C.; Eigenthaler, U.; Weigand, M.; Schutz, G. Rapid Prototyping of Fresnel Zone Plates via Direct Ga^+ Ion Beam Lithography for High-Resolution X-Ray Imaging. *ACS Nano* **2013**, *7*, 9788−9797.
(16) Allen, F. I. Branched High Aspect Ratio Nanostructures Fabricated by Focused Helium Ion Beam Induced Deposition of an Insulator. *Micromachines* **2021**, *12*, No. 232, DOI: 10.3390/mi12030232.
(17) Manoccio, M.; Esposito, M.; Passaseo, A.; Cuscuna, M.; Tasco, V. Focused Ion Beam Processing for 3D Chiral Photonics Nanostructures. *Micromachines* **2021**, *12*, No. 6, DOI: 10.3390/mi12010006.
(18) Córdoba, R.; Orus, P.; Strohauer, S.; Torres, T. E.; De Teresa, J. M. Ultra-Fast Direct Growth of Metallic Micro- and Nano-Structures by Focused Ion Beam Irradiation. *Sci. Rep.* **2019**, *9*, No. 14076.
(19) Bret, T.; Hofmann, T.; Edinger, K. Industrial Perspective on Focused Electron Beam-Induced Processes. *Appl. Phys. A* **2014**, *117*, 1607−1614.
(20) Choi, W.; Kim, C.; Kang, H. Interactions of Low Energy (10−600 ev) Noble Gas Ions with a Graphite Surface: Surface Penetration, Trapping and Self-Sputtering Behaviors. *Surf. Sci.* **1993**, *281*, 323−335, DOI: 10.1016/0039-6028(93)90645-Z.
(21) Joy, D. C. *Helium Ion Microscopy Principles and Applications*; Springer, 2013.
(22) Chen, P. A.; Alkemade, P. F. A.; Salemink, H. W. M. The Complex Mechanisms of Ion-Beam-Induced Deposition. *Jpn. J. Appl. Phys.* **2008**, *47*, No. 5123, DOI: 10.1143/JJAP.47.5123.
(23) Alkemade, P. F. A.; Miro, H. Focused Helium-Ion-Beam-Induced Deposition. *Appl. Phys. A* **2014**, *117*, 1727−1747.
(24) Indrajith, S.; Rousseau, P.; Huber, B. A.; Nicolafrancesco, C.; Domaracka, A.; Grygoryeva, K.; Nag, P.; Sedmidubská, B.; Fedor, J.; Kočišek, J. Decomposition of Iron Pentacarbonyl Induced by Singly and Multiply Charged Ions and Implications for Focused Ion Beam-Induced Deposition. *J. Phys. Chem. C* **2019**, *123*, 10639−10645.
(25) Thorman, R. M.; Kumar, T. P. R.; Fairbrother, D. H.; Ingolfsson, O. The Role of Low-Energy Electrons in Focused Electron Beam Induced Deposition: Four Case Studies of Representative Precursors. *Beilstein J. Nanotechnol.* **2015**, *6*, 1904−1926.
(26) De Teresa, J. M.; Córdoba, R.; Fernández-Pacheco, A.; Montero, O.; Strichovanec, P.; Ibarra, M. R. Origin of the Difference in the Resistivity of As-Grown Focused-Ion- and Focused-Electron-Beam-Induced Pt Nanodeposits. *J. Nanomater.* **2009**, *2009*, No. 936863, DOI: 10.1155/2009/936863.
(27) Li, Y.; Xu, S.; Sezen, M.; Misirlioglu, F. B.; Vredenbregt, E. J. D. Rubidium Focused Ion Beam Induced Platinum Deposition. *J. Vac. Sci. Technol. B* **2023**, *41*, No. 042803, DOI: 10.1116/6.0002609.
(28) Puretz, J.; Swanson, L. W. Focused Ion Beam Deposition of Pt Containing Films. *J. Vac. Sci. Technol., B: Microelectron. Nanometer Struct. Process., Meas., Phenom.* **1992**, *10*, 2695−2698.
(29) Steele, A. V.; Schwarzkopf, A.; McClelland, J. J.; Knuffman, B. High-Brightness Cs Focused Ion Beam from a Cold-Atomic-Beam Ion Source. *Nano Futures* **2017**, *1*, No. 015005.
(30) Tao, T.; Ro, J.; Melngailis, J.; et al. Focused Ion Beam Induced Deposition of Platinum. *J. Vac. Sci. Technol., B: Microelectron. Process. Phenom.* **1990**, *8*, 1826−1829, DOI: 10.1116/1.585167.
(31) Telari, K. A.; Rogers, B. R.; Fang, H.; Shen, L.; Weller, R. A.; Braski, D. N. Characterization of Platinum Films Deposited by Focused Ion Beam-Assisted Chemical Vapor Deposition. *J. Vac. Sci. Technol., B: Microelectron. Nanometer Struct. Process., Meas., Phenom.* **2002**, *20*, 590−595.
(32) ten Haaf, G.; Wouters, S. H. W.; van der Geer, S. B.; Vredenbregt, E. J. D.; Mutsaers, P. H. A. Performance Predictions of a Focused Ion Beam from a Laser Cooled and Compressed Atomic Beam. *J. Appl. Phys.* **2014**, *116*, No. 244301.
(33) Salvador-Porroche, A.; Sangiao, S.; Philipp, P.; Cea, P.; Teresa, J. M. Optimization of Pt-C Deposits by Cryo-FIBID: Substantial Growth Rate Increase and Quasi-Metallic Behaviour. *Nanomaterials* **2020**, *10*, No. 1906, DOI: 10.3390/nano10101906.
(34) Shedd, G. M.; Lezec, H.; Dubner, A. D.; Melngailis, J. Focused Ion Beam Induced Deposition of Gold. *Appl. Phys. Lett.* **1986**, *49*, 1584−1586.
(35) *Ion Beam Modification of Solids*; Springer International Publishing: Switzerland, 2016.
(36) Wnuk, J. D.; Gorham, J. M.; Rosenberg, S. G.; van Dorp, W. F.; Madey, T. E.; Hagen, C. W.; Fairbrother, D. H. Electron Induced Surface Reactions of the Organometallic Precursor Trimethyl-(Methylcyclopentadienyl)Platinum(IV). *J. Phys. Chem. C* **2009**, *113*, 2487−2496, DOI: 10.1021/jp807824c.
(37) Moulder, J. F.; Stickle, W. F.; Sobol, P. E.; Bomben, K. D. *Handbook of X-Ray Photoelectron Spectroscopy*; Perkin Elmer Corporation: Eden Prarie, MN, 1992.
(38) Feng, X.; Abdel-Rahman, M. K.; Kruppe, C. M.; Trenary, M. Deposition and Characterization of Stoichiometric Films of V_2O_5 on Pd(111). *Surf. Sci.* **2017**, *664*, 1−7, DOI: 10.1016/j.susc.2017.05.004.
(39) Landheer, K.; Rosenberg, S. G.; Bernau, L.; Swiderek, P.; Utke, I.; Hagen, C. W.; Fairbrother, D. H. Low-Energy Electron-Induced Decomposition and Reactions of Adsorbed Tetrakis-(trifluorophosphine)platinum $[Pt(PF_3)_4]$. *J. Phys. Chem. C* **2011**, *115*, 17452−17463.
(40) Agarwal, S.; Lin, Y.; Li, C.; Stoller, R. E.; Zinkle, S. J. On the Use of SRIM for Calculating Vacancy Production: Quick Calculation and Full-Cascade Options. *Nucl. Instrum. Methods Phys. Res., Sect. B* **2021**, *503*, 11−29.
(41) Goethel, P. J.; Yang, R. T. Platinum-Catalyzed Hydrogenation of Graphite: Mechanism Studied by the Rates of Monolayer Channeling. *J. Catal.* **1986**, *101*, 342−351.
(42) Menon, P. G.; Froment, G. F. Modification of the Properties of Pt-AI_2O_3 Catalysts by Hydrogen at High Temperatures. *J. Catal.* **1979**, *59*, 138−147.
(43) Menon, P. G.; Froment, G. F. Residual Hydrogen in Supported Platinum Catalysts and Its Influence on Their Catalytic Properties. *Appl. Catal.* **1981**, *1*, 31−48.
(44) Miller, J. T.; Myers, B. L.; Modica, F. S.; Lane, G. S.; Vaarkamp, M.; Koningsberger, D. C. Hydrogen Temperature Programmed Desorption (H_2 TPD) of Supported Platinum Catalysts. *J. Catal.* **1993**, *143*, 395−408.
(45) Tillekaratne, A.; Trenary, M. Adsorption and Dehydrogenation of Decaborane on the Pt(111) Surface. *J. Phys. Chem. C* **2009**, *113*, 13847−13854.
(46) Orús, P.; Sigloch, F.; Sangiao, S.; De Teresa, J. M. Cryo-Focused Ion Beam-Induced Deposition of Tungsten-Carbon Nanostructures Using a Thermoelectric Plate. *Appl. Sci.* **2021**, *11*, No. 10123, DOI: 10.3390/app112110123.
(47) Belianinov, A.; Burch, M. J.; Ievlev, A.; Kim, S.; Stanford, M. G.; Mahady, K.; Lewis, B. B.; Fowlkes, J. D.; Rack, P. D.;

Ovchinnikova, O. S. Direct Write of 3D Nanoscale Mesh Objects with Platinum Precursor via Focused Helium Ion Beam Induced Deposition. *Micromachines* **2020**, *11*, No. 527, DOI: 10.3390/mi11050527.

(48) Prestigiacomo, M.; Roussel, L.; Houël, A.; Sudraud, P.; Bedu, F.; Tonneau, D.; Safarov, V.; Dallaporta, H. Studies of Structures Elaborated by Focused Ion Beam Induced Deposition. *Microelectron. Eng.* **2004**, *76*, 175−181.

(49) Sigmund, P.; Szymonski, M. Temperature-Dependent Sputtering of Metals and Insulators. *Appl. Phys. A: Solids Surf.* **1984**, *33*, 141−152.

(50) Besocke, K.; Berger, S.; Hofer, W. O.; Littmark, U. A search for a thermal spike effect in sputtering. I. Temperature Dependence of the Yield at Low-kev, Heavy-Ion Bombardment. *Radiat. Eff.* **1982**, *66*, 35−41.

(51) Botman, A.; Mulders, J. J. L.; Weemaes, R.; Mentink, S. Purification of Platinum and Gold Structures After Electron-Beam-Induced Deposition. *Nanotechnology* **2006**, *17*, 3779−3785.

(52) Ghosh, S.; Avasthi, D. K.; Tripathi, A.; Kabiraj, D.; Singh, S.; Misra, D. S. Electronic Sputtering of Carbon Allotropes. *Nucl. Instrum. Methods Phys. Res., Sect. B* **2004**, *219−220*, 973−979, DOI: 10.1016/j.nimb.2004.01.199.

https://doi.org/10.1021/acs.jpcc.4c00630
J. Phys. Chem. C 2024, 128, 7723−7732